

The proton radius and its relatives - much ado about nothing?

Ulf-G. Meißner

HISKP and BCTP, Bonn University, D-53115 Bonn, Germany
IKP-3 and IAS-4, Forschungszentrum Jülich, D-52425 Jülich, Germany
Tbilisi State University, 0186 Tbilisi, Georgia

E-mail: meissner@hiskp.uni-bonn.de

Abstract. I summarize the dispersion-theoretical analysis of the nucleon electromagnetic form factors. Special emphasis is given on the extraction of the proton charge radius and its relatives, the proton magnetic radius as well as the neutron magnetic radius. Some recent work on the hyperfine splitting in leptonic hydrogen and on radiative corrections to muon-proton scattering is also discussed. Some views on future studies are given.

1. Introduction

The measurement of the 2S-2P energy splitting in muonic hydrogen by the CREMA collaboration with 10^{-5} relative accuracy [1, 2] started the so-called “proton radius puzzle”, as the then accepted value from electron-proton scattering was significantly larger, see e.g. [3], contrasting the “small radius” $r_E^p \simeq 0.84$ fm with the “large” one, $r_E^p \simeq 0.88$ fm. This stirred lots of activities, both on the experimental as well as on the theoretical side, see e.g. the recent reviews [4, 5]. However, as I will show in this talk, the dispersion-theoretical analysis of the ep scattering data and the available data for the form factors from data in the timelike region always led to the small radius and continues to do so. In fact, the radius puzzle was anticipated in 2007 in Ref. [6], where it was shown that the DR analysis of ep scattering could not accommodate the then accepted radius from the Lamb shift in electronic hydrogen of $r_E^p = 0.88 - 0.89$ fm. Without going into further details of this intriguing story, that is, without telling about all the twists and turns (or: confusions and errors) that appeared over time, I will illuminate some developments that were not appreciated by large parts of the community for a long time. More precisely, what I will show here is that the powerful approach of dispersion relations (DRs), that allows one to include all possible physics constraints, is arguably the best method to analyze the data that are sensitive to the nucleons electromagnetic form factors and thus the various sizes of the nucleon as given by the electric and magnetic radii of the proton and the neutron.

2. Formalism

First, let me define the nucleon electromagnetic form factors. For the dispersive analysis it is mandatory to consider protons and neutrons together, for details see the review [7]. These form factors are given by the matrix element of the electromagnetic current j_μ^{em} sandwiched between

nucleon states,

$$\langle p' | j_\mu^{\text{em}} | p \rangle = \bar{u}(p') \left[F_1(t) \gamma_\mu + i \frac{F_2(t)}{2m} \sigma_{\mu\nu} q^\nu \right] u(p), \quad (1)$$

with m the nucleon mass (either proton or neutron), $u(p)$ a conventional nucleon spinor and $t = (p' - p)^2$ the four-momentum transfer squared. In the space-like region, one often uses the variable $Q^2 = -t > 0$. The form factors are normalized as $F_1^p(0) = 1$, $F_1^n(0) = 0$, $F_2^p(0) = \kappa_p$ and $F_2^n(0) = \kappa_n$, with $\kappa_p = 1.793$ and $\kappa_n = -1.913$ the anomalous magnetic moment of the proton and the neutron, respectively. Also used are the Sachs (electric and magnetic) form factors, given by $G_E(t) = F_1(t) - \tau F_2(t)$, $G_M(t) = F_1(t) + F_2(t)$, with $\tau = -t/(4m^2)$. The proton charge radius and the corresponding magnetic radius follow as

$$(r_E^p)^2 = 6 \frac{dG_p^E(t)}{dt} \Big|_{t=0}, \quad (r_M^p)^2 = \frac{6}{\mu_p} \frac{dG_p^M(t)}{dt} \Big|_{t=0}, \quad (2)$$

with $\mu_p = 1 + \kappa_p$. The neutron radii are defined similarly, note, however, that $G_E^n(0) = 0$.

Next, we turn to the dispersive analysis of the nucleon electromagnetic form factors. For a generic form factor $F(t)$, one writes down an unsubtracted dispersion relation of the form:

$$F(t) = \frac{1}{\pi} \int_{t_0}^{\infty} \frac{\text{Im} F(t')}{t' - t - i\epsilon} dt'. \quad (3)$$

Here, t_0 is the threshold of the lowest cut of $F(t)$ and the $i\epsilon$ defines the integral for values of t on the cut. In fact, in the isospin basis, $t_0 = 4M_\pi^2$ in the isovector and $t_0 = 9M_\pi^2$ in the isoscalar channel, respectively. The imaginary part $\text{Im} F$, the so-called *spectral function*, encodes the constraints from analyticity and unitarity besides other important physics. These spectral functions are given in terms of continua, narrow vector meson poles as well as broad vector mesons. In the isovector case, the spectral function can be reconstructed up to about $t \simeq 1 \text{ GeV}^2$ from data on pion-nucleon scattering and the pion vector form factor, as pioneered in Ref. [8] and most precisely done in Ref. [9]. This in fact not only generates the ρ -meson but also an important enhancement on the left shoulder of the ρ , that is of utmost importance to properly describe the nucleon isovector radii [10]. In the isoscalar spectral function, the ω -meson represents the lowest contribution. It is not affected by uncorrelated three-pion exchange [11]. Further up, in the region of the ϕ -meson, there is a strong competition between $K\bar{K}$ and $\pi\rho$ effects, which to some extent suppresses this part of the spectral function. For momenta above $t \simeq 1 \text{ GeV}^2$, effective narrow poles represent the physics at higher energies. To describe the observed oscillations of the cross sections for $e^+e^- \rightarrow p\bar{p}$ and $e^+e^- \rightarrow n\bar{n}$ in the timelike region, additional broad poles are required. The spectral functions are further constrained by the normalizations of the form factors as well as the perturbative QCD behavior, $F_1(t) \sim 1/t^2$ and $F_2(t) \sim 1/t^3$. A cartoon of the spectral functions is given in Fig. 1.

The spectral functions are determined from a fit to the world data set on electron-proton scattering as well as the reactions $e^+e^- \leftrightarrow \bar{p}p, \bar{n}n$, the latter giving the form factors in the timelike region. The fit parameters are the vector meson masses (except for the ω and the ϕ) and the residua as well as the widths for the broad poles. There are two sources of uncertainties that need to be accounted for. First, the statistical error is obtained using a bootstrap procedure and second, the systematic error is calculated from varying the number of vector meson poles so that the total χ^2 does not change by more than 1% [12]. A detailed description of these methods is given in the review [7].

3. Results for the form factors

Fitting to the world data basis of data in the spacelike and the timelike regions (about 1800 data points), the form factors are obtained with good precision. Details of these fits are given

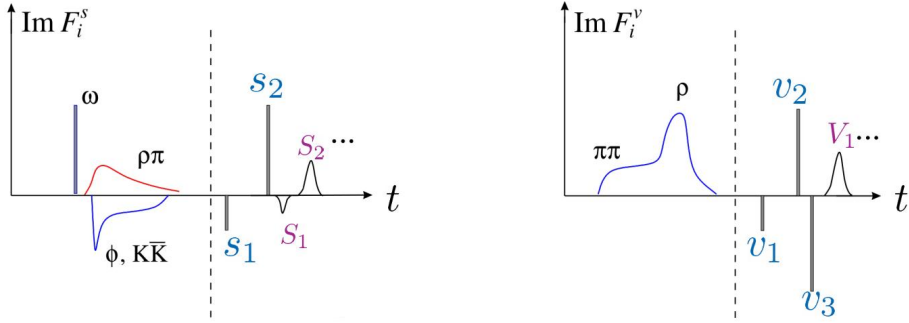


Figure 1. Sketch of the isoscalar (left) and isovector (right) spectral function. In the left panel, the ω and ϕ mesons are relevant together with the $\pi\rho$ and $K\bar{K}$ continua, while s_1, s_2, \dots are narrow and S_1, S_2, \dots are broad effective poles. In the right panel, the $\pi\pi$ continuum not only generates the ρ but is also visibly enhanced on the left shoulder of the ρ . Further, v_1, v_2, v_3, \dots are narrow and V_1, \dots are broad effective poles.

in Ref. [13]. The electric and magnetic form factors of the proton in the spacelike region from Ref. [13] normalized to the canonical dipole form, $G_{\text{dip}}(Q^2) = (1 + Q^2/0.71 \text{ GeV}^2)^{-2}$, are shown in Fig. 2 together with their statistical and systematic uncertainties. It is interesting to note that the form factor ratio $\mu_p G_E^p(Q^2)/G_M^p(Q^2)$ measured at Jefferson Lab seems to level off with increasing momentum transfer, somewhat disfavoring a zero crossing. To settle this issues certainly requires more measurements extending to $Q^2 \simeq 10 \text{ GeV}^2$. Predictions for the upcoming PRad-II experiment at Jefferson Lab are made in Ref. [14].

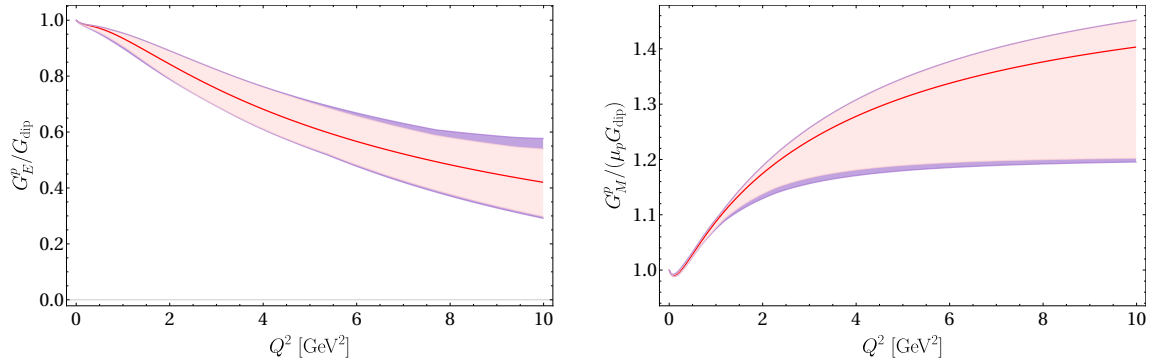


Figure 2. Electric (left panel) and magnetic (right panel) form factor of the proton from Ref. [13] divided by the canonical dipole form factor are shown by the red lines. The light red band is the statistical uncertainty and the purple band shows the systematic error added in quadrature.

The form factors in the timelike region are complex-valued quantities. In most experiments, the modulus of the effective form factor $|G_{\text{eff}}(t)|$ is extracted, which is a linear combination of $|G_E(t)|$ and $|G_M(t)|$, see e.g. [7, 15] for definitions. There are clearly visible oscillations, which in the DR approach are generated by the interference of the broad poles. However, there are other mechanisms proposed to generate such structures, see e.g. Refs. [16, 17, 18, 19, 20].

4. Results for the radii

From the just discussed form factors, the extracted proton radii are [13]

$$r_E^p = 0.840^{+0.003+0.002}_{-0.002-0.002} \text{ fm} , \quad r_M^p = 0.849^{+0.003+0.001}_{-0.003-0.004} \text{ fm} , \quad (4)$$

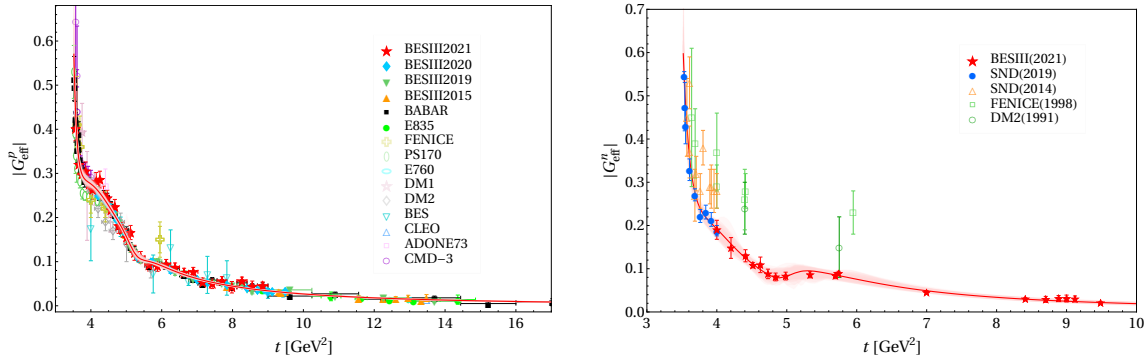


Figure 3. Oscillations in the proton (left panel) and neutron (right panel) effective form factor in the timelike region from the complete fit to all data [13]. Closed symbols are fitted and open symbols are not fitted. The complete data basis is given in Ref. [13].

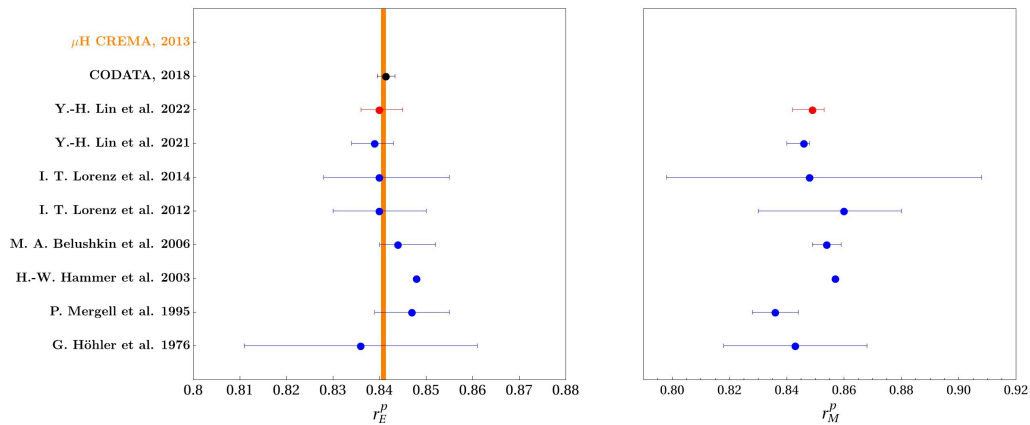


Figure 4. DR determinations of the proton charge radius (left panel) and the proton magnetic radius (right panel). Also shown are the CREMA result and the CODATA 2018 value for r_E^p . Values are in [fm]. References from top to bottom: [2, 21, 13, 22, 18, 23, 6, 24, 25, 12].

where the first error is statistical and the second one systematic. This value of the proton charge radius is consistent with recent experimental determination as shown in Tab. 1 and the present CODATA value of 0.8414(19) fm. Other recent determinations of the proton charge radius give $r_E^p = 0.842(10)$ fm [26], 0.847(8) fm [27] and 0.852(9) fm [28] and for the magnetic radius $r_M^p = 0.850(10)$ fm [26], 0.739(41) fm [29] and 0.817(27) fm [30]. For more discussion on these determinations, see Ref. [22]. As further shown in Fig. 4, the proton charge and magnetic radius have been rather stable since the 1976 Karlsruhe DR [12], with $r_M^p > r_E^p$ always.

Let me now consider the neutron radii. The charge radius squared is used as input in most DR analyses, with the exception of Ref. [6], where it was also extracted (and came out consistent with other determinations). In the most recent analysis, the precise value extracted from ed scattering using chiral nuclear EFT was used, $(r_E^n)^2 = -0.105^{+0.005}_{-0.006}$ fm² [36]. The extracted magnetic radius for the neutron is

$$r_M^n = 0.864^{+0.004+0.006}_{-0.004-0.001} \text{ fm} . \quad (5)$$

The uncertainties are a bit larger than for the proton, but in any case, the neutron magnetic radius is the largest of all, $r_M^n > r_M^p > r_E^p$, and it has been equally constant over time as shown in Fig. 5. For comparison, Ref. [29] gives $r_M^n = 0.878(79)$ fm. I mention that the bump-dip structure seen at low Q^2 in $G_M^n(Q^2)$ in some form factor extractions is inconsistent with the

Table 1. Recent determination of the proton charge radius from the electronic Lamb shift in hydrogen (H) and ep scattering compared to the most recent DR result.

r_E^p [fm]	year	method	Ref.
0.877(13)	2018	H Lamb shift	[31]
0.833(10)	2019	H Lamb shift	[32]
0.8482(38)	2020	H Lamb shift	[33]
0.8584(51)	2021	H Lamb shift	[34]
0.831(7)(12)	2019	ep scattering	[35]
0.840(3)(2)	2022	DR	[13]

restrictions from analyticity and unitarity, as such a structure would require a vector meson with a mass of about 400 MeV that is excluded by the spectral functions shown above.

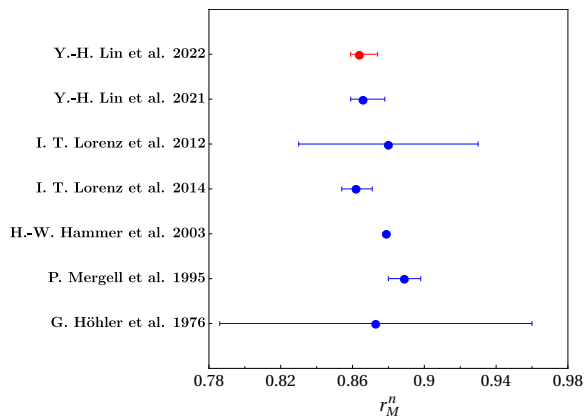


Figure 5. Extraction of the neutron magnetic radius r_M^n in units of fm based on dispersion-theoretical analyses since 1976. References as in Fig. 4.

Finally, it is interesting to compare the DR results with recent lattice QCD determinations. In Tab. 2, the isovector radii are displayed as these are free of disconnected diagrams. Only simulations at the physical pion mass are considered. While the isovector electric radius appears to converge to the DR result, the situation is less clear in the isovector magnetic case. Clearly, more precise lattice studies need to be performed.

Table 2. Recent determination of the nucleon isovector radii from lattice QCD simulations with physical pion masses.

	r_E^V [fm]	r_M^V [fm]
DR [13]	0.900(2)(2)	0.854(1)(3)
Lattice/Mainz (2021) [37]	0.894(14)(12)	0.813(18)(7)
Lattice/ETMC (2020) [38]	0.827(47)(5)	—
Lattice/PACS (2019) [39]	0.785(17)(21)	0.758(33)(286)
Lattice/MIT (2018) [40]	0.787(87)	—

5. Remarks on the hyperfine-splitting in leptonic hydrogen

Laser spectroscopy of muonic hydrogen (μH), an atom formed by a negatively charged muon and a proton, represents an excellent pathway to investigate low-energy properties of the proton. While the 2S-2P energy splitting is sensitive to electric properties of the proton as the proton

charge radius as discussed before, the hyperfine splitting (HFS) is sensitive also to magnetic properties of the proton as it arises from the interaction between the proton and muon magnetic moments. For recent reviews, see Refs. [41, 42]. For the HFS, the leading proton structure contribution is given by the two-photon-exchange contribution $\Delta E^{2\gamma}$, which is conventionally divided into a Zemach radius contribution $\Delta_Z^{\mu\text{H}}$, a recoil contribution $\Delta_{\text{recoil}}^{\mu\text{H}}$ and a polarizability contribution $\Delta_{\text{pol}}^{\mu\text{H}}$ [43, 44, 46, 45, 47, 48]. The Zemach contribution $\Delta_Z^{\mu\text{H}}$ that accounts for the elastic part of the two-photon exchange contribution can be expressed through the electric and magnetic Sachs form factors of the proton [49]

$$\Delta_Z = -2Z\alpha m_r r_Z^p, \quad r_Z^p = -\frac{4}{\pi} \int_0^\infty \frac{dQ}{Q^2} \left[\frac{G_E^p(Q^2)G_M^p(Q^2)}{1 + \kappa_p} - 1 \right], \quad (6)$$

where Z is the atomic number, $\alpha = e^2/(4\pi)$ the electromagnetic fine-structure constant, μ_r the reduced mass of the lepton-proton system and r_Z^p is the Zemach radius. The so-called recoil contribution, which more precisely is the recoil correction to the Zemach contribution, can also be described solely by form factors. In addition to the Sachs form factors in this case also the Dirac and Pauli form factors enter [42]:

$$\Delta_{\text{recoil}} = \frac{Z\alpha}{\pi(1 + \kappa_p)} \int_0^\infty \frac{dQ}{Q} \left\{ \frac{G_M^p(Q^2)}{Q^2} \frac{8m_l m_p}{v_l + v_p} \left(2F_1^p(Q^2) + \frac{F_1^p(Q^2) + 3F_2^p(Q^2)}{(v_l + 1)(v_p + 1)} \right) - \frac{8m_r G_M^p(Q^2)G_E^p(Q^2)}{Q} - \frac{m_l (F_2^p)^2(Q^2)}{m_p} \frac{5 + 4v_l}{(1 + v_l)^2} \right\}, \quad (7)$$

where $v_p = (1 + 4m_p^2/Q^2)^{1/2}$, $v_l = (1 + 4m_l^2/Q^2)^{1/2}$ and m_p (m_l) is the proton (lepton) mass. A precise evaluation of $\Delta_{\text{recoil}}^{\mu\text{H}}$ is timely given the ongoing experimental efforts carried out by three collaborations that aim at the HFS in μH [50, 51, 52] with relative accuracies ranging from 1 to 10 ppm.

Based on the form factors from [13], the Zemach radius is:

$$r_Z^p = 1.054_{-0.002}^{+0.003+0.000} \text{ fm}, \quad (8)$$

which is compared to earlier determinations in Fig. 6.

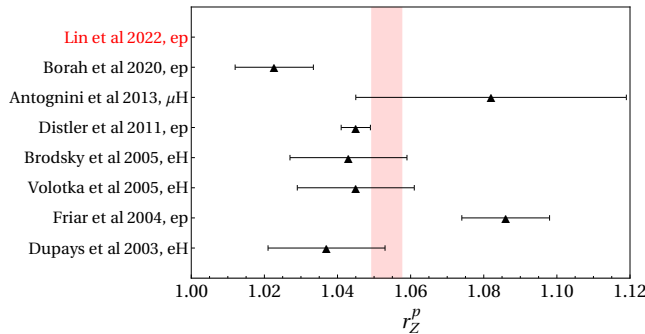


Figure 6. Extraction of the Zemach radius (in units of fm) from various methods (*ep* scattering, electronic hydrogen and muonic hydrogen). References from top to bottom: [13, 29, 2, 53, 54, 55, 56, 57].

Consider now the calculation of the recoil correction defined in Eq. (7) using the form factors from [13]. For the μH system, this gives [58]

$$\Delta_{\text{recoil}}^{\mu\text{H}} = (837.6_{-1.0}^{+1.7+2.2}) \times 10^{-6} = (837.6_{-1.0}^{+2.8}) \times 10^{-6} = (837.6_{-1.0}^{+2.8}) \text{ ppm}, \quad (9)$$

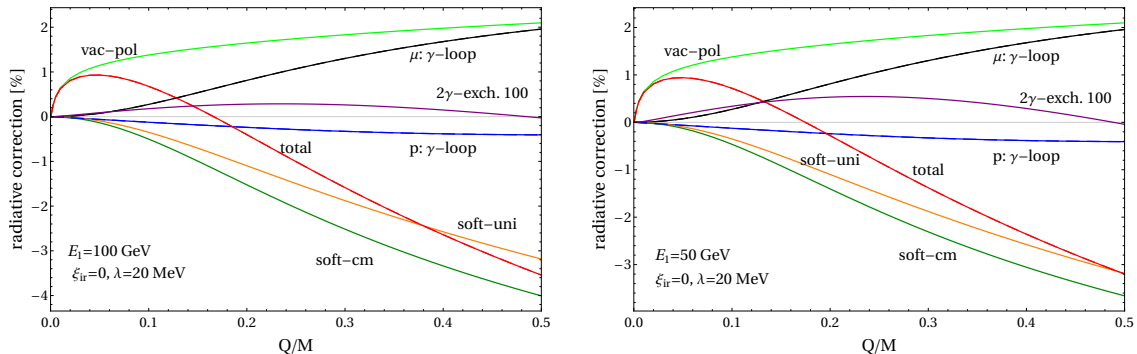


Figure 7. Radiative corrections for the AMBER kinematics with $E_1 = 100$ GeV (left panel) and $E_1 = 50$ GeV (right panel). The individual radiative corrections from vacuum polarization, the virtual photon-loops and soft bremsstrahlung are shown together with their sum, see the solid line labeled “total”.

with the first/second error is the statistical/systematic uncertainty. These errors are a few per mille, so that this can be considered as a high-precision determination. Compared with the most recent value from Ref. [46], $\Delta_{\text{recoil}}^{\mu\text{H}} = 844(7) \times 10^{-6}$, these numbers agree within errors but the new result is more precise. The analogous value for regular hydrogen (eH) is [58]

$$\Delta_{\text{recoil}}^{e\text{H}} = (526.9_{-0.3}^{+1.1+1.3}) \times 10^{-8} = (526.9_{-0.4}^{+1.7}) \times 10^{-8}, \quad (10)$$

which is, as expected, two orders of magnitude smaller but with comparable uncertainties as in the μH case. Again, the corresponding value from Ref. [46], $\Delta_{\text{recoil}}^{e\text{H}} = 532.8(4.9) \times 10^{-8}$, is about 1% larger but is also a bit less precise. For further discussion, see Ref. [58].

6. Remarks on muon-proton scattering

Elastic muon-proton scattering at low momentum transfers offers an alternative method to measure the proton charge radius r_E^p . Any deviation from the value measured in ep scattering would challenge the concept of lepton-flavor universality, which is a cornerstone of the so successful Standard Model of particle physics, that was put into question in recent experiments on certain decay modes of B mesons. There are experiments that are pursuing such proton radius measurements, namely MUSE at PSI [59] and AMBER at CERN [60]. Both experiments were triggered by the abovementioned proton radius discrepancy. In Ref. [61] the radiative corrections to $\mu^\mp p$ scattering specifically for the kinematics of the AMBER experiment, which operates with a high-energetic muon beam at 100 GeV and measures in near forward directions, thus spanning the momentum transfers $32 \text{ MeV} < Q < 141 \text{ MeV}$, were worked out. This momentum transfer range nicely overlaps with the range of the upcoming MUSE experiment at PSI with $45 \text{ MeV} < Q < 265 \text{ MeV}$, the PRAD-II experiment at Jefferson Lab for e^-p scattering with $14 \text{ MeV} < Q < 245 \text{ MeV}$ [62] as well as the MAGIC e^-p experiment at Mainz, that aims at a momentum range $10 \text{ MeV} < Q < 292 \text{ MeV}$ [63]. The AMBER experiment intends to measure the proton radius with an accuracy of better than 0.01 fm, which requires a detailed study of the radiative corrections to be able to achieve such an accuracy. For related work on radiative corrections to μp scattering, see Refs. [64, 65, 41].

Based on earlier works [66, 67], Ref. [61] provided an update on the radiative corrections for the AMBER experiment based on the high-precision form factors from [13]. In Fig. 7 the radiative corrections from all sources of order α/π for the planned AMBER experiment with a muon beam energy of $E_1 = 100$ GeV and for $E_1 = 50$ GeV are shown, assuming an infrared cutoff of $\lambda = 20$ MeV. At small momentum transfers $Q/M \lesssim 0.06$, vacuum polarization is the

most dominant effect, because it is driven by the electron mass scale. After that, the soft-photon radiation takes over, with a sizable contribution (of 2%) from the photon-loop form factor $2F_1^{\gamma\text{-fin}}$, involving the muon mass scale, at the upper end of the momentum transfers considered here. The negative photon-loop form factor contribution from the proton stays below 0.4% in magnitude, and the two-photon exchange correction of maximal size $0.3 \cdot 10^{-4}$ can essentially be neglected. It can be seen that for the ratio to the Born cross section, only the minor terms from the photon-loop form factors of the proton and two-photon exchange depend on the proton structure predetermined by the strong interactions. Since a prominent role among the radiative corrections is played by soft photon radiation, the calculation of the bremsstrahlung process $\mu p \rightarrow \mu p \gamma$ should be extended beyond the soft photon approximation and tailored to the specific experimental conditions. Such work is under way.

7. Final thoughts

DRs are arguably the best tool to analyze the electromagnetic form factors of the nucleon as they allow for a consistent description of all data in the space- and timelike regions based on fundamental principles. DR analyses always led to a small proton charge radius and a slightly bigger magnetic one. Also, most recent experiments tend to the small radius, so the attention has turned from a puzzle to precision [68]. Also consistently over time, the neutron magnetic radius has been and is the largest of the electromagnetic nucleon radii. Even more precise measurements of ep scattering at Jefferson Lab and Mainz are eagerly awaited for as well as refined lattice QCD calculations. Theory challenges are the consistent extraction of the neutron form factors from light nuclei along the lines of Ref. [36] and to obtain a better understanding of the oscillations in the effective form factors $|G_{\text{eff}}^{p,n}|$. Experimental challenges are a measurement of the proton form factor ratio at $Q^2 \simeq 10 \text{ GeV}^2$, more resolved form factor measurements in the timelike region and the investigation of μp scattering (MUSE, AMBER) to test lepton flavor universality.

Acknowledgments

First, I would like to thank the organizers of INPC 2022 for their superb job done. Second, I would like to thank my collaborators Yong-Hui Lin, Hans-Werner Hammer, Norbert Kaiser and Aldo Antognini for sharing their insights into the topics discussed here. This work is supported in part by the DFG (Project number 196253076 - TRR 110) and the NSFC (Grant No. 11621131001) through the funds provided to the Sino-German CRC 110 ‘‘Symmetries and the Emergence of Structure in QCD’’, by the European Research Council (ERC) under the European Union’s Horizon 2020 research and innovation programme (EXOTIC, grant agreement No. 101018170), by the Chinese Academy of Sciences (CAS) through a President’s International Fellowship Initiative (PIFI) (Grant No. 2018DM0034) and by the VolkswagenStiftung (Grant No. 93562).

References

- [1] R. Pohl *et al.*, *Nature* **466** (2010), 213-216.
- [2] A. Antognini *et al.*, *Science* **339** (2013), 417-420.
- [3] J. C. Bernauer *et al.* [A1], *Phys. Rev. C* **90** (2014) 015206.
- [4] J. P. Karr, D. Marchand and E. Voutier, *Nature Rev. Phys.* **2** (2020) 601-614.
- [5] H. Gao and M. Vanderhaeghen, *Rev. Mod. Phys.* **94** (2022) 015002.
- [6] M. A. Belushkin, H. W. Hammer and U.-G. Meißner, *Phys. Rev. C* **75** (2007) 035202.
- [7] Y. H. Lin, H. W. Hammer and U.-G. Meißner, *Eur. Phys. J. A* **57** (2021) 255.
- [8] W. R. Frazer and J. R. Fulco, *Phys. Rev. Lett.* **2** (1959) 365.
- [9] M. Hoferichter *et al.*, *Eur. Phys. J. A* **52** (2016) 331.
- [10] G. Höhler and E. Pietarinen, *Phys. Lett. B* **53** (1975) 471-475.
- [11] V. Bernard, N. Kaiser and U.-G. Meißner, *Nucl. Phys. A* **611** (1996) 429-441.

- [12] G. Höhler *et al.*, Nucl. Phys. B **114** (1976) 505-534.
- [13] Y. H. Lin, H. W. Hammer and U.-G. Meißner, Phys. Rev. Lett. **128** (2022) 052002.
- [14] Y. H. Lin, H. W. Hammer and U.-G. Meißner, Phys. Lett. B **827** (2022) 136981.
- [15] S. Pacetti, R. Baldini Ferroli and E. Tomasi-Gustafsson, Phys. Rept. **550-551** (2015) 1-103.
- [16] A. Bianconi and E. Tomasi-Gustafsson, Phys. Rev. Lett. **114** (2015) 232301.
- [17] A. Bianconi and E. Tomasi-Gustafsson, Phys. Rev. C **93** (2016) 035201.
- [18] I. T. Lorenz, U.-G. Meißner, H. W. Hammer and Y. B. Dong, Phys. Rev. D **91** (2015) 014023.
- [19] E. Tomasi-Gustafsson, A. Bianconi and S. Pacetti, Phys. Rev. C **103** (2021) 035203.
- [20] Q. H. Yang *et al.*, [arXiv:2206.01494 [nucl-th]].
- [21] E. Tiesinga, P. J. Mohr, D. B. Newell and B. N. Taylor, Rev. Mod. Phys. **93** (2021) 025010.
- [22] Y. H. Lin, H. W. Hammer and U.-G. Meißner, Phys. Lett. B **816** (2021) 136254.
- [23] I. T. Lorenz, H. W. Hammer and U.-G. Meißner, Eur. Phys. J. A **48** (2012) 151.
- [24] H. W. Hammer and U.-G. Meißner, Eur. Phys. J. A **20** (2004) 469-473.
- [25] P. Mergell, U.-G. Meißner and D. Drechsel, Nucl. Phys. A **596** (1996) 367-396.
- [26] J. M. Alarcón, D. W. Higinbotham and C. Weiss, Phys. Rev. C **102** (2020) 035203.
- [27] Z. F. Cui, D. Binosi, C. D. Roberts and S. M. Schmidt, Phys. Rev. Lett. **127** (2021) 092001.
- [28] H. Atac, M. Constantinou, Z.-E. Meziani, M. Paolone and N. Sparveris, Eur. Phys. J. A **57** (2021) 65.
- [29] K. Borah, R. J. Hill, G. Lee and O. Tomalak, Phys. Rev. D **102** (2020) 074012.
- [30] Z. F. Cui, D. Binosi, C. D. Roberts and S. M. Schmidt, Chin. Phys. Lett. **38** (2021) 121401.
- [31] H. Fleurbaey *et al.*, Phys. Rev. Lett. **120** (2018) 183001.
- [32] N. Bezginov *et al.*, Science **365** (2019) 1007-1012.
- [33] A. Grinin *et al.*, Science **370** (2020) 1061-1066.
- [34] A. D. Brandt *et al.*, Phys. Rev. Lett. **128** (2022) 023001.
- [35] W. Xiong *et al.*, Nature **575** (2019) 147-150.
- [36] A. A. Filin *et al.*, Phys. Rev. C **103** (2021) 024313.
- [37] D. Djukanovic *et al.*, Phys. Rev. D **103** (2021) 094522.
- [38] C. Alexandrou *et al.*, Phys. Rev. D **101** (2020) 114504.
- [39] E. Shintani *et al.*, Phys. Rev. D **99** (2019) 014510 [erratum: Phys. Rev. D **102** (2020) no.1, 019902].
- [40] N. Hasan *et al.*, Phys. Rev. D **97** (2018) 034504.
- [41] C. Peset, A. Pineda and O. Tomalak, Prog. Part. Nucl. Phys. **121** (2021) 103901.
- [42] A. Antognini, F. Hagelstein and V. Pascalutsa, [arXiv:2205.10076 [nucl-th]].
- [43] C. E. Carlson, V. Nazaryan and K. Griffioen, Phys. Rev. A **78** (2008) 022517.
- [44] C. E. Carlson, V. Nazaryan and K. Griffioen, Phys. Rev. A **83** (2011) 042509.
- [45] O. Tomalak, Eur. Phys. J. C **77** (2017) 517.
- [46] O. Tomalak, Eur. Phys. J. A **54** (2018) 3.
- [47] R. N. Faustov, I. V. Gorbacheva and A. P. Martynenko, Proc. SPIE Int. Soc. Opt. Eng. **6165** (2006) 0M.
- [48] F. Hagelstein, R. Miskimen and V. Pascalutsa, Prog. Part. Nucl. Phys. **88** (2016) 29.
- [49] A. C. Zemach, Phys. Rev. **104** (1956) 1771-1781.
- [50] P. Amaro *et al.*, [arXiv:2112.00138 [physics.atom-ph]].
- [51] S. Kanda *et al.* Phys. Lett. B **815** (2021) 136154.
- [52] C. Pizzolotto *et al.*, Eur. Phys. J. A **56** (2020) 185.
- [53] M. O. Distler, J. C. Bernauer and T. Walcher, Phys. Lett. B **696** (2011) 343-347.
- [54] S. J. Brodsky *et al.*, Phys. Rev. Lett. **94** (2005) 022001 [erratum: Phys. Rev. Lett. **94** (2005) 169902].
- [55] A. V. Volotka, V. M. Shabaev, G. Plunien and G. Soff, Eur. Phys. J. D **33** (2005) 23-27.
- [56] J. L. Friar and I. Sick, Phys. Lett. B **579** (2004) 285-289.
- [57] A. Dupays, A. Beswick, B. Lepetit, C. Rizzo and D. Bakalov, Phys. Rev. A **68** (2003) 052503.
- [58] A. Antognini, Y. H. Lin and U.-G. Meißner, [arXiv:2208.04025 [nucl-th]].
- [59] E. J. Downie [MUSE], EPJ Web Conf. **73** 07005 (2014).
- [60] B. Adams *et al.* [arXiv:1808.00848 [hep-ex]].
- [61] N. Kaiser, Y. H. Lin and U.-G. Meißner, Phys. Rev. D **105** (2022) 076006.
- [62] A. Gasparian *et al.* [PRad], [arXiv:2009.10510 [nucl-ex]].
- [63] A. Denig, J. Univ. Sci. Tech. China **46** (2016) 608-616.
- [64] O. Tomalak and M. Vanderhaeghen, Eur. Phys. J. C **76** (2016) 125.
- [65] O. Tomalak and M. Vanderhaeghen, Eur. Phys. J. C **78** (2018) 514.
- [66] N. Kaiser, J. Phys. G **37** (2010) 115005.
- [67] N. Kaiser, J. Phys. G **44** (2017) 055003.
- [68] H. W. Hammer and U.-G. Meißner, Sci. Bull. **65** (2020) 257-258.